

Confinement Effect Driven Quantum Spin Hall Effect in Monolayer AuTe₂Cl

Guyue Zhong,^{1,*} Q. Xie,¹ and Gang Xu^{1,†}

¹Wuhan National High Magnetic Field Center and School of Physics,
Huazhong University of Science and Technology, Wuhan 430074, China

(Dated: June 13, 2021)

Based on first-principles calculations, we predict that the monolayer AuTe₂Cl is a quantum spin Hall (QSH) insulator with a topological band gap about 10 meV. The three-dimensional (3D) AuTe₂Cl is a topological semimetal that can be viewed as the monolayer stacking along **b** axis. By studying the energy level distribution of *p* orbitals of Te atoms for the bulk and the monolayer, we find that the confinement effect driven $p_y^- - p_z^+$ band inversion is responsible for the topological nontrivial nature of monolayer. Since 3D bulk AuTe₂Cl has already been experimentally synthesized, we expect that monolayer AuTe₂Cl can be exfoliated from a bulk sample and the predicted QSH effect can be observed.

PACS numbers:

INTRODUCTION

Two-dimensional (2D) topological insulators (TIs), known as quantum spin Hall (QSH) insulators are characterized by a topological nontrivial bulk gap and gapless helical edge states protected by time-reversal symmetry from backscattering at the sample boundaries [1–3]. Because of their potential applications in semiconductor spintronics, they have recently attracted great attention in condensed matter physics [4]. For example, the QSH edge channels may be useful for applications in integrated circuit technology, where power dissipation is becoming a more and more serious problem as devices becoming smaller. Up to now, the QSH effect only has been observed in HgTe/CdTe [5, 6], InAs/GaSb [7, 8] quantum wells and WTe₂ [9] under low temperature and ultrahigh vacuum, which hinder their applications in realistic devices. To overcome the thermal disturbance and promote the practical application of QSH insulators, those materials containing heavy atoms with extremely strong spin-orbital coupling (SOC), such as MX (M = Zr, Hf and X = Cl, Br, I) [10], MTe₅ (M = Zr, Hf) [11], BiTeI [12], have been extensively studied. These results demonstrate that those 2D materials are good candidates to realize the QSH effect at room temperature. In spite of those progresses, desirable materials preferably with high feasibility of experimental realization are still extremely scarce and deserve to explore in experiment and theory.

Recently, the catalogue of topological electronic materials greatly enriches the number of new topological materials, which has listed all 3D TIs and topological semimetals (TSMs) based on symmetry indicators [13–15], and inspires the enthusiasm for the study of new topological materials. As we know, some 3D TIs and TSMs are closely related to 2D QSH insulators [16]. They can be built up by stacking 2D QSH insulating layers along a certain crystal orientation while the QSH effect can be achieved in an exfoliated, monolayer TI and TSM. A well-studied example is transition metal

dichalcogenides 1T'-MX₂ (M = W, Mo and X = S, Se, Te) [17]. This is a new way to search for new layered materials from the catalogue of topological electronic materials and study the two-dimensional topological nature to achieve QSH effect.

In this paper, we study the structure and electronic properties of bulk and monolayer AuTe₂Cl. We find that the bulk AuTe₂Cl is a TSM with a band inversion along Γ –Y direction. While the monolayer is a QSH insulator with a $p_y^- - p_z^+$ band inversion at the $\bar{\Gamma}$ point in the 2D BZ. This band inversion is driven by the confinement effect, which eliminates the coupling between p_y orbitals along *y* direction and pulls down the anti-bonding state p_y^- below the Fermi level and the bonding state p_z^+ . Its topological nontrivial nature is demonstrated through the Wannier center evolution and surface density of state (DOS) calculations. Therefore, we present a new way of exploring 2D QSH insulators from 3D TSMs. We expect the predicted AuTe₂Cl monolayer and its QSH effect can be realized in future experiments.

METHODS

First-principles calculations based on density functional theory (DFT) are carried out by the Vienna *ab initio* simulation package (VASP) [18–20]. The exchange-correlation functional is treated within the local-density approximation (LDA) [21]. A self-consistent field method (tolerance 10^{-5} eV/atom) is employed in conjunction with plane-wave basis sets of cutoff energy of 500 eV. Atomic structure optimization is implemented until the remanent Hellmann-Feynman forces on the ions are less than 0.01 eV/Å. We use $11 \times 11 \times 7$ and $11 \times 1 \times 7$ Γ -centered **k**-meshes to sample the BZ of bulk and monolayer systems, respectively. The vacuum layer is set to 15 Å to minimize artificial interaction between layers. SOC is considered for all calculations. For monolayer, we also perform hybrid functions calculations to correct

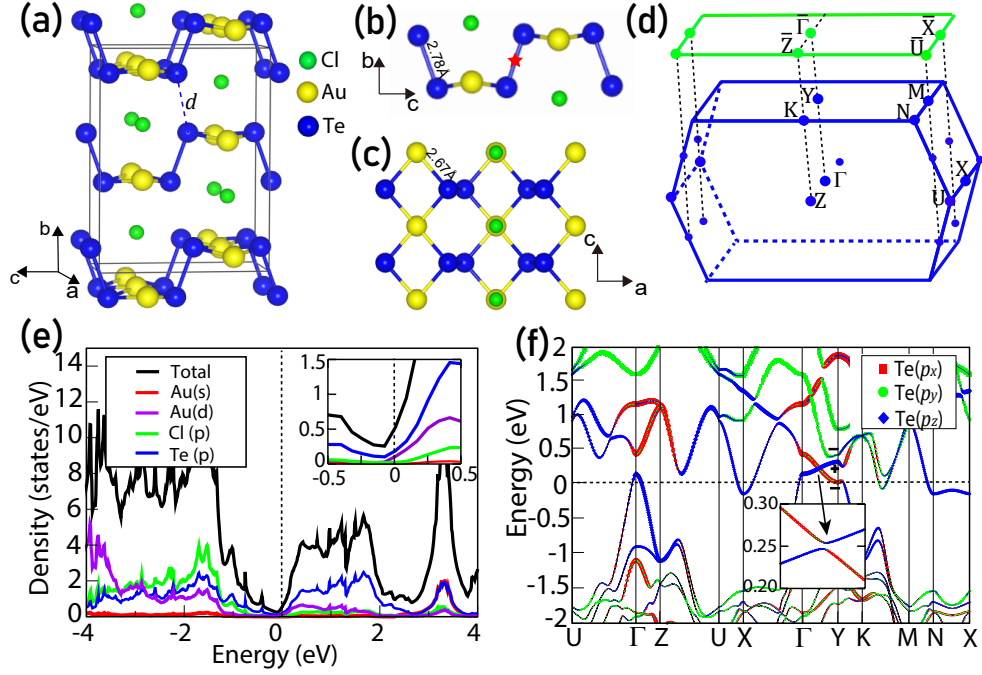


FIG. 1: (a) The crystal structure of bulk AuTe₂Cl. It has a layered orthorhombic structure and d is the distance of two adjacent layers. (b), (c) are the side view and top view of the AuTe₂Cl monolayer, respectively. The red star in (b) denotes an inversion center. (d) The 3D Brillouin zone for the bulk and the 2D BZ for the monolayer with high symmetry k points labeled. (e) The total DOS and projected DOS for bulk AuTe₂Cl. (f) The projected band structure for the three p orbitals of Te in the bulk AuTe₂Cl. The size of the red squares, green circles and blue diamonds represent the weight of p_x , p_y and p_z orbitals, respectively.

its band structure [22]. The maximum localized Wannier functions are constructed by using the Wannier90 package [23]. The topological properties are calculated by using Wanniertools [24].

RESULTS AND DISCUSSION

The bulk compound AuTe₂Cl has been synthesized in experiment [25–27], which adopts a layered orthorhombic structure (D_{2h} point group) and lattice constant $a = 4.02$ Å, $b = 11.87$ Å, $c = 8.77$ Å with the nonsymmorphic space group $Cmcm$ (No. 63), as shown in Fig. 1(a). For each layer, a pair of Te atoms is joined to neighboring Au atoms and forms a Au-Te-Te-Au corrugated net, which is sandwiched by the upper and lower Cl atoms. Therefore, each Au atom is coordinated with four Te atoms and, likewise, each Te atom is coordinated with four Au atoms. The bond length of Au-Te and Te-Te covalent bond are 2.67 Å and 2.78 Å, respectively. The short bond length indicates that strong covalent bonds are formed and, are responsible for the in-plane crystal stability. The interaction along b axis are mainly contributed by the Te-Te bond (3.2 Å) between two adjacent layers [see d in Fig. 1(a)]. The Te-Te bonds along b axis are much weaker than the covalent bonds in the xz plane, which means it is experimentally possible to

exfoliated monolayer AuTe₂Cl from bulk samples [see Figs. 1(b) and 1(c)]. The interlayer coupling strength of AuTe₂Cl is similar to the cases of GeSe and SnSe [28], but stronger than typical van der Waals materials, such as graphite [29] and 2H-MoS₂ [30].

From the projected density of states (PDOS) of bulk AuTe₂Cl shown in Fig. 1(e), we observe that the most important orbitals within the energy window from -1.2 to 2.0 eV are the Te p orbitals. The Au d orbitals and Cl p orbitals mainly contribute to the states below -1.2 eV, and the Au s orbitals are responsible for the peak at 3.4 eV. From these observation, we can understand the electronic transfer and chemical bonding as follows. Each Au atom donates a $5s$ electron to the Cl $3p$ empty orbitals, which lowers the total energy and keeps the PDOS of these orbitals away from the Fermi level. The band structure of bulk system in Fig. 1(f) reveals a semimetal character, where the valence band is partially empty resulting in a hole pocket along Γ –Y, while the conduction band is partially filled resulting in an electron pocket along X–M. This has been confirmed in transport experiments [27]. When the SOC is neglected, there is a Dirac point along Γ –Y direction at 0.25 eV above the Fermi level formed by the p_x and p_z band crossing. When SOC is considered, a topological nontrivial gap about 7 meV is opened up. The parities of (p_x, p_y, p_z) orbitals at Γ (and Y) point are $(-, -, +)$, respectively, as shown in Fig. 1(f). For the

covalent bonding between p orbitals, the bonding state has the positive parity and the anti-bonding state has the negative parity. Therefore, the p_z orbitals are bonding states and the p_x , p_y orbitals are anti-bonding states near the Fermi level. We notice that the p_y orbitals have a stronger dispersion along Γ –Y direction compared with p_x and p_z orbitals, which is mainly due to the relatively strong hopping between p_y orbitals along y -direction.

Now we focus on the topological properties of monolayer system. Due to relatively strong coupling of p_y orbitals in the y direction, when bulk AuTe₂Cl is exfoliated to the monolayer, the confinement effect should be considered. We simulate the transform from bulk to monolayer by increasing the adjacent layer distance d . Fig. 2(a) exhibits the evolution of conduction band minimum (CBM) of p_x and p_y orbitals, and valance band maximum (VBM) of p_z orbitals at Y point with increasing d . It demonstrates that the CBM of the p_y orbitals rapidly falls below the p_x orbitals and the Fermi level. While the CBM of p_x and the VBM of p_z orbitals rise slightly. When $d > 4.2$ Å, the energy levels of three p orbitals reach stationary values, indicating vanishing of the interlayer coupling along y direction. Moreover, when the d is large enough, the band dispersion along Γ –Y disappears, which means the system reach its monolayer limit. Hence the topological nature is determined by the $\bar{\Gamma}$ point in the 2D BZ.

To illustrate the band inversion process in the monolayer AuTe₂Cl explicitly, we start from the Te p orbitals and consider the effect of chemical bonding and confinement effect for bulk and monolayer AuTe₂Cl. This is schematically depicted in the three stages in Fig. 2(b). Stage I represents the chemical bonding process between Te atoms. As analysed above, the states around the Fermi energy are mainly contributed by bonding states of Te p_z orbitals with positive parity $\xi = +1$ and anti-bonding states of p_x and p_y orbitals with negative parity $\xi = -1$. At this stage, the bonding states have lower energy below Fermi level and the anti-bonding states have higher energy above the Fermi level. In stage II, the energy levels have changed mainly due to hopping along y direction. The band inversion occurs between the p_x orbitals with parity $\xi = -1$ and the p_z orbitals with parity $\xi = +1$. Stage III represents the rearrangement of energy levels driven by the confinement effect. Since p_y orbitals have larger hopping constants along the y direction, the confinement effect will influence p_y orbitals much stronger than the p_x and p_z orbitals, and pulls down the p_y orbitals below the Fermi level. As a result, the band inversion happens between the bonding state of p_z orbitals and the anti-bonding state of p_y orbitals in the monolayer AuTe₂Cl.

In order to obtain a stable monolayer structure, the lattice parameters and ions positions are fully optimized in the LDA calculation. The total energy with respect to the lattice constants are given in Fig. 2(c). The lowest to-

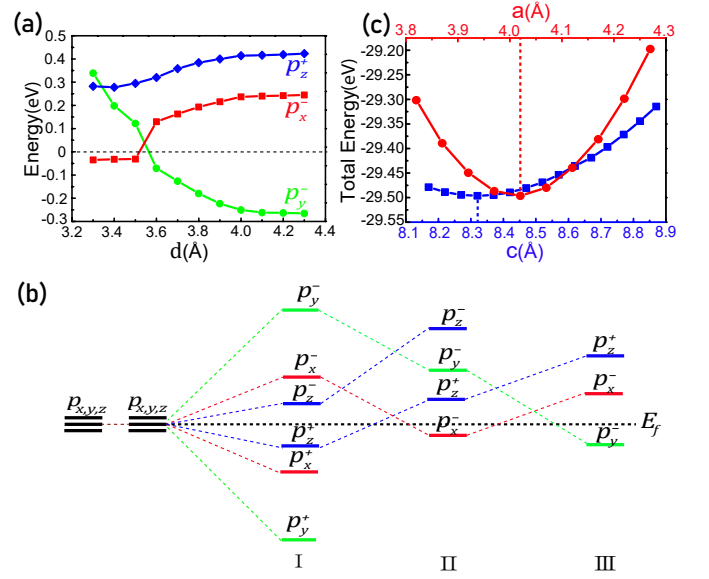


FIG. 2: (a) The evolution of the energy level of the three p orbitals of Te, respectively, with increasing d . (b) The chemical bonding and confinement effect on the p orbitals are schematically represented. I: The three p orbitals form bonding and anti-bonding states. II: The energy level evolution due to hopping along y direction. The band inversion happens between p_x^+ and p_z^- . III: The confinement effect lower the p_y^- state and results in a $p_y^- - p_z^+$ band inversion at $\bar{\Gamma}$ point. (c) The total energy curves with respect to lattice parameters a and c , respectively. The energy minimum corresponds to $a = 4.02$ Å and $c = 8.32$ Å.

tal energy corresponds to $a = 4.02$ Å and $c = 8.32$ Å. The LDA band structure of monolayer AuTe₂Cl is shown in Fig. 3(a). In the absence of SOC, the monolayer AuTe₂Cl shows semimetal feature with a Dirac point located on the $\bar{\Gamma}$ – \bar{X} path in the 2D BZ, which confirms the band inversion at $\bar{\Gamma}$ point. When the SOC is considered, the Dirac point is gapped out. Our LDA results suggest that the monolayer AuTe₂Cl is very close to an insulating state. The overlap between the CBM and VBM is about 27 meV. We further perform the hybrid functional calculations using the HSE06 functional. The HSE06 band structure exhibits a positive band gap about 10 meV at the Fermi level, as shown in Fig. 3(b). This means when interlayer distance d is increased, the system undergoes a topological semimetal to topological insulator phase transition.

Since monolayer AuTe₂Cl has inversion symmetry, the Z_2 topological invariant can be determined by the parities of all occupied bands at the four time-reversal-invariant-momentum (TRIM) points. According to Fu-Kane formula, $(-1)^v = \prod_i \delta_i$ with $\delta_i = \prod_{m=1}^N \xi_{2m}(\Gamma_i)$. Here v is the Z_2 number and $\xi_{2m}(\Gamma_i)$ is the parity of the $2m$ th occupied band at TRIM point Γ_i [31]. For monolayer AuTe₂Cl, the calculated δ_i for four TRIM points $\bar{\Gamma}$, \bar{Y} , \bar{X} and \bar{U} are given by $-$, $-$, $-$, $+$, respectively.

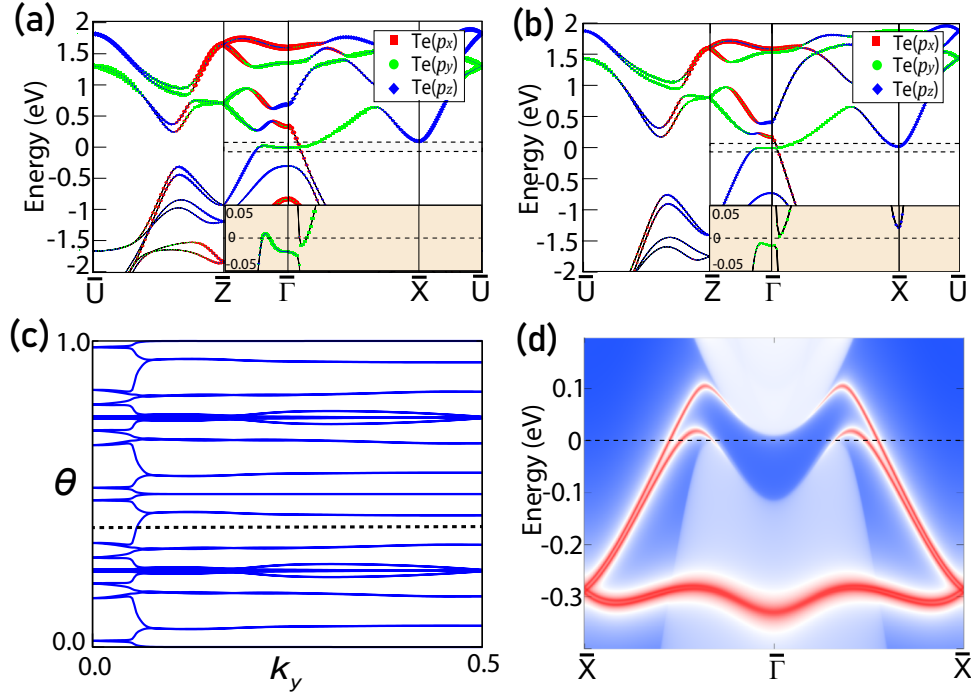


FIG. 3: Results for the monolayer AuTe_2Cl . (a), (b) are the band structures from LDA and hybrid functional calculations, respectively. In each case, the p orbitals of Te are projected out. (c) The Wannier center evolution in the y -direction with the SOC calculation. The reference dash line crosses the evolution line once which indicates a topological nontrivial band structure. (d) The surface DOS along $\bar{X} - \bar{\Gamma}$ of the 2D BZ. The red topological edge states are clearly visible.

Hence the Z_2 number $\nu = 1$, which demonstrates that it is a topological nontrivial insulator. The topological nontrivial nature can also be confirmed by the calculated Wannier center evolution as shown in Fig. 3(c). The reference dash line crosses the evolution line an odd number of times in the y -direction. We also calculate the edge spectrum in Fig. 3(d), in which pair of gapless edge states connects the conduction bands and the valence bands. From all these compelling evidences, we thus conclude that the monolayer AuTe_2Cl is a QSH insulator with a topological band gap about 10 meV. It should be noted that the 3D bulk AuTe_2Cl has been experimentally synthesized [25–27]. We expect the monolayer system can be exfoliated from its 3D counterpart, or from molecular beam epitaxy growth method.

In summary, we predict that the monolayer AuTe_2Cl is a QSH insulator with a topological band gap about 10 meV. The nontrivial band topology stems from the band inversion between p_y anti-bonding state and p_z bonding state of Te atoms at $\bar{\Gamma}$ point. This band inversion is driven by the confinement effect when 3D bulk system is exfoliated to monolayer thickness. Since bulk AuTe_2Cl has been experimentally synthesized, we expect the experimental realization of monolayer AuTe_2Cl and the predicted QSH effect are also very promising. Our work demonstrates how 2D QSH insulators can be de-

signed from 3D layered TSMs or TIs. This may further promote the exploration of 2D TIs.

ACKNOWLEDGEMENTS

The authors thank Shuang Jia for fruitful discussion. This work is supported by the Ministry of Science and Technology of China (No. 2018YFA0307000) and the National Natural Science Foundation of China (No. 11874022).

* Electronic address: gyzhong@hust.edu.cn

† Electronic address: gangxu@hust.edu.cn

- [1] M. Z. Hasan and C. L. Kane. *Colloquium: Topological insulators*. *Rev. Mod. Phys.* 82, 3045-3067, 2010.
- [2] Xiao-Liang Qi and Shou-Cheng Zhang. Topological insulators and superconductors. *Rev. Mod. Phys.* 83, 1057-1110, 2011
- [3] Binghai Yan and Shou-Cheng Zhang. Topological materials. *Rep. Prog. Phys.* 75, 096501, 2012.
- [4] Lukas Mühler, Haijun Zhang, Stanislav Chadov, Binghai Yan, Frederick Casper, Jürgen Kübler, Shou-Cheng Zhang and Claudia Felser. Topological Insulators from a Chemist's Perspective. *Angew. Chem.* 124, 7333-7337, 2012.

- [5] B. Andrei Bernevig, Taylor L. Hughes and Shou-Cheng Zhang. Quantum Spin Hall Effect and Topological Phase Transition in HgTe Quantum Wells. *Science* 314, 1757, 2012.
- [6] Markus König, Steffen Wiedmann, Christoph Brüne, Andreas Roth, Hartmut Buhmann, Laurens W. Molenkamp, Xiao-Liang Qi and Shou-Cheng Zhang. Quantum Spin Hall Insulator State in HgTe Quantum Wells. *Science* 318, 766-770, 2007.
- [7] Chaoxing Liu, Taylor L. Hughes, Xiao-Liang Qi, Kang Wang and Shou-Cheng Zhang. Quantum Spin Hall Effect in Inverted Type-II Semiconductors. *Phys. Rev. Lett.* 100, 236601, 2008.
- [8] Ivan Knez, Rui-Rui Du and Gerard Sullivan. Evidence for Helical Edge Modes in Inverted InAs/GaSb Quantum Wells. *Phys. Rev. Lett.* 107, 136603, 2011.
- [9] Sanfeng Wu, Valla Fatemi, Quinn D. Gibson, Kenji Watanabe, Takashi Taniguchi, Robert J. Cave and Pablo Jarillo-Herrero. Observation of the quantum spin Hall effect up to 100 kelvin in a monolayer crystal. *Science*, 359, 76-79, 2018.
- [10] Liujiang Zhou, Liangzhi Kou, Yan Sun, Claudia Felser, Feiming Hu, Guangcun Shan, Sean C. Smith, Binghai Yan and Thomas Frauenheim. New Family of Quantum Spin Hall Insulators in Two-dimensional Transition-Metal Halide with Large Nontrivial Band Gaps. *Nano Lett.*, 15, 7867-7872, 2015.
- [11] Hongming Weng, Xi Dai and Zhong Fang. Transition-Metal Pentatelluride $ZrTe_5$ and $HfTe_5$: A Paradigm for Large-Gap Quantum Spin Hall Insulators. *Phys. Rev. X*. 4, 011002, 2014.
- [12] M.S. Bahrany, B.-J. Yang, R. Arita and N. Nagaosa. Emergence of non-centrosymmetric topological insulating phase in BiTeI under pressure. *Nat. Commun.* 3, 679, 2012.
- [13] Tiantian Zhang, Yi Jiang, Zhida Song, He Huang, Yuqing He, Zhong Fang, Hongming Weng and Chen Fang. Catalogue of topological electronic materials. *Nature* 566, 475-479, 2019.
- [14] M.G. Vergniory, L. Elcoro, Claudia Felser, Nicolas Regnault, B. Andrei Bernevig, Zhijun Wang. A complete catalogue of high-quality topological materials. *Nature* 566, 480-485, 2019.
- [15] Feng Tang, Hoi Chun Po, Ashvin Vishwanath and Xiang-gang Wan. Efficient topological materials discovery using symmetry indicators. *Nature Physics* 15, 470-476, 2019.
- [16] Hongming Weng, Rui Yu, Xiao Hu, Xi Dai and Zhong Fang. Quantum anomalous Hall effect and related topological electronic states. *Advances in Physics* 64, 227-282, 2015.
- [17] Xiaofeng Qian, Junwei Liu, Liang Fu, Ju Li. Quantum spin Hall effect in two-dimensional transition metal dichalcogenides. *Science*, 346, 1344-1347, 2015.
- [18] G. Kresse and J. Furthmüller. Efficient iterative schemes for ab initio total-energy calculations using a plane-wave basis set. *Phys. Rev. B* 54, 11169-11186, 1996.
- [19] G. Kresse and J. Hafner. Ab initio molecular dynamics for open-shell transition metals. *Phys. Rev. B* 48, 13115-13118, 1993.
- [20] G. Kresse and D. Joubert. From ultrasoft pseudopotentials to the projector augmented-wave method. *Phys. Rev. B* 59, 1758-1775, 1999.
- [21] J. P. Perdew and Alex Zunger. Self-interaction correction to density-functional approximations for many-electron systems. *Phys. Rev. B* 23, 5048-5079, 1981.
- [22] Jochen Heyd and Gustavo E. Scuseria. Hybrid functionals based on a screened Coulomb potential. *J. Chem. Phys.* 118, 8207, 2015.
- [23] Arash A. Mostofi, Jonathan R. Yates, Giovanni Pizzi, Young-Su Lee, Ivo Souza, David Vanderbilt and Nicola Marzari. An updated version of wannier90: A tool for obtaining maximally-localised Wannier functions. *Comput. Phys. Commun.* 185, 2309-2310, 2014.
- [24] QuanSheng Wu, ShengNan Zhang, Hai-Feng Song, Matthias Troyer and Alexey A. Soluyanov. WannierTools: An open-source software package for novel topological materials. *Comput. Phys. Commun.* 224, 405-416, 2018.
- [25] H.M. Haendler, D. Mootz, A. Rabenau and G. Rosenstein. The crystal structures of $AuTe_2Cl$ and $AuTe_2I$. *J. Solid State Chem.* 10, 175, 1974.
- [26] B L Zhou, E Gmelin and R Villar. Determination of the Fermi surface of $AuTe_2Br$ by Shubnikov-de Haas effect. *J. Phys. C: Solid State Phys* 14, 4393, 1981.
- [27] Zeji Wang, Shuyu Cheng, Tay-Rong Chang, Wenlong Ma, Xitong Xu, Huibin Zhou, Guangqiang Wang, Xin Gui, Haipeng Zhu, Zhen Zhu, Hao Zheng, Jinfeng Jia, Junfeng Wang, Weiwei Xie, and Shuang Jia. Highly Mobile Carriers in a Candidate of Quasi-Two-Dimensional Topological Semimetal $AuTe_2Br$. arXiv:1909.04296v1 10 Sep 2019.
- [28] M. Taniguchi, R. L. Johnson, J. Ghijsen, and M. Cardona. Core excitons and conduction-band structures in orthorhombic GeS, GeSe, SnS, and SnSe single crystals. *Phys. Rev. B* 42, 3634-3643, 1990.
- [29] B. T. Kelly. Physics of graphite. *United Kingdom: Applied Science* 1981.
- [30] Andrea Splendiani, Liang Sun, Yuanbo Zhang, Tianshu Li, Jonghwan Kim, Chi-Yung Chim, Giulia Galli and Feng Wang. Emerging Photoluminescence in Monolayer MoS_2 . *Nano Lett.* 10, 1271-1275, 2010.
- [31] Liang Fu and C. L. Kane. Topological insulators with inversion symmetry. *Phys. Rev. B* 76, 045302, 2015.